OPEN

High-Accuracy Nodal Staging of Head and Neck Cancer With USPIO-Enhanced MRI

A New Reading Algorithm Based on Node-to-Node Matched Histopathology

Daphne A.J.J. Driessen, MD, Patrik Zámecnik, MD,† Tim Dijkema, MD, PhD,* Sjoert A.H. Pegge, MD,† Adriana C.H. van Engen-van Grunsven, MD, PhD,‡ Robert P. Takes, MD, PhD,§ Johannes H.A.M. Kaanders, MD, PhD,* and Tom W.J. Scheenen, PhD†*

Abstract:

Objectives: Ultrasmall superparamagnetic iron oxide (USPIO)–enhanced magnetic resonance imaging (MRI) is a potential diagnostic tool for lymph node assessment in patients with head and neck cancer. Validation by radiologic-pathologic correlation is essential before the method is evaluated in clinical studies. In this study, MRI signal intensity patterns of lymph nodes are correlated to their histopathology to develop a new USPIO-enhanced MRI reading algorithm that can be used for nodal assessment in head and neck cancer patients.

Materials and Methods: Ten head and neck cancer patients underwent in vivo USPIO-enhanced MRI before neck dissection. An ex vivo MRI of the neck dissection specimen was performed for precise coregistration of in vivo MRI with histopathology. Normal clinical histopathological workup was extended with meticulous matching of all lymph nodes regarded as potentially metastatic based on their in vivo MRI signal intensity pattern. On the basis of histopathology of resected nodes, in vivo MRI signal characteristics were defined separating benign from malignant lymph nodes.

Results: Fifteen of 34 node-to-node correlated lymph nodes with remaining signal intensity on T2*-weighted MRI were histopathologically metastatic and 19 were benign. Radiological analysis revealed that metastatic lymph nodes showed equal or higher MRI signal intensity when compared with lipid tissue on T2*-weighted MGRE sequence (15/16 lymph nodes; 94%), whereas healthy lymph nodes showed lower (17/19 lymph nodes; 89%) or complete attenuation of signal intensity (273/279; 98%) when compared with lipid tissue on T2*-weighted MGRE. Histopathology of all resected specimens identified 392 lymph nodes. Six lymph nodes with (micro)metastases were missed with in vivo MRI. Whether these 6 lymph nodes were correlated to a nonmalignant lymph node on in vivo MRI or could not be detected at all is unclear.

Conclusions: We developed a new reading algorithm to differentiate benign from malignant lymph nodes in head and neck cancer patients on the basis of their appearance on high-resolution T2*-weighted USPIO-enhanced MRI. Next steps involve validation of our reading algorithm to further improve the accuracy of neck lymph node staging with USPIO-enhanced MRI in prospective clinical studies with larger number of patients.

Key Words: lymph node metastases, ultrasmall superparamagnetic iron oxide, magnetic resonance imaging, reading algorithm, head and neck cancer

(*Invest Radiol* 2022;57: 810–818)

The importance of accurate nodal evaluation in head and neck cancer has been stressed throughout literature. Metastatic lymph node involvement is associated with an increased recurrence rate and a decreased survival.[1] The accuracy of current imaging modalities remains insufficient since approximately 20% of patients with a clinically (ie, palpably and radiologically) negative neck harbor occult metastases.[2,3] Clinically node-negative patients are usually treated electively (surgery or radiotherapy) to eradicate this subclinical disease. However, in the majority of these patients, elective neck treatment is futile as they are free of occult disease. This results in unnecessary morbidity with permanent deleterious effects on the quality of life.

The diagnostic potential of ultrasmall superparamagnetic iron oxide (USPIO) nanoparticles used as a magnetic resonance imaging (MRI) contrast agent to detect small metastatic deposits in lymph nodes has gained renewed interest after its reintroduction in 2014.[4–7] The presence or absence of USPIO deposits can be visualized with 3-dimensional (3D) iron-sensitive, T2*-weighted MRI at a high spatial resolution. The nanoparticles are taken up by cells of the mononuclear phagocyte system and accumulate in healthy (parts of) lymph nodes, attenuating MR signal due to their paramagnetic effects. In metastatic lymph nodes, USPIO uptake is restrained resulting in MR signal preservation.[8] USPIO-enhanced MRI to differentiate between healthy and suspicious pelvic lymph nodes has been widely studied in prostate cancer patients and demonstrated improved sensitivity when compared with conventional MRI (90.5% vs 35.4%) and computed tomography (CT) (83% vs 34%).[9,10] In the years 2000–2011, comparable results have been reported for head and neck cancer.[11–18] However, the available data are sparse and outdated since the contrast agent was withdrawn from the market authorization application in 2007 and reintroduced in 2014.[6,19] Moreover, MR methodology has improved since and therefore urges reevaluation of the technique.[20] In addition, there is a possible difference in the MR appearance of the pelvic and head and neck lymph nodes: lymph nodes draining the oral and pharyngeal mucosa are frequently subjected to inflammatory changes, potentially modifying USPIO uptake due to postinflammatory fibrosis or high amounts of inflammatory cells in the lymph nodes. Consequently, the evaluation algorithm of the head and neck lymph nodes using USPIO-enhanced MRI could differ from the pelvic lymph nodes, and therefore, the previously described evaluation algorithm for the pelvic lymph nodes on multislice 2-dimensional (2D) image acquisitions

Received for publication March 29, 2022; and accepted for publication, after revision, May 18, 2022.

From the Departments of *Radiation Oncology, †Medical Imaging, ‡Pathology, and §Otorhinolaryngology and Head and Neck Surgery, Radboud University Medical Center, Nijmegen, the Netherlands.

Correspondence to: Daphne A.J.J. Driessen, MD, Department of Radiation Oncology, Radboud University Medical Center, Geert Grooteplein 32, 6525 AG Nijmegen, the Netherlands. E-mail: daphne.driessen@radboudumc.nl.

Conflicts of interest and sources of funding: P.Z. declares to be a "Scientific Advisor to SPL Medical B.V." and owner of options of SPL Medical B.V. The other authors declare that they have no conflicts of interest with the content of this article.

The research project was funded by the Radboud Institute for Health Sciences junior research grant obtained in 2017. The funding body had no role in the design of the study and collection, analysis, and interpretation of data and in the writing of the manuscript.

Supplemental digital contents are available for this article. Direct URL citations appear in the printed text and are provided in the HTML and PDF versions of this article on the journal's Web site (www.investigativeradiology.com).

ISSN: 0020-9996/22/5712–0810

DOI: 10.1097/RLI.0000000000000902

cannot simply be copied.[9,21–23] To identify distinctive MRI nodal characteristics for detection and differentiation of benign and malignant lymph nodes in patients diagnosed with head and neck cancer, a direct correlation between in vivo MRI features of these nodes on USPIO-enhanced MRI and histopathological findings is crucial.

Therefore, we initiated the USPIO-NECK study (ClinicalTrials.gov Identifier NCT03817307), which aims to evaluate the use of modern high-resolution 3D USPIO-enhanced MRI for nodal staging in head and neck cancer. The first aim of this study, which is presented in this article, was to develop a radiological reading algorithm for USPIO-enhanced MRI for head and neck lymph node staging on the basis of step-section histopathology of resected and node-to-node matched (from in vivo to histopathology) lymph nodes. This step is necessary to conduct the second part of the study with a larger number of patients, which aims at validation of the new algorithm.

MATERIALS AND METHODS

Ethical Considerations

This prospective single-center explorative study was carried out after approval of the institutional ethics committee. Written informed consent was obtained from all participants.

Patients

Between April 2019 and October 2020, 11 patients were enrolled in the study. Subjects were eligible to participate if the following inclusion criteria were met: (1) age ≥18 years; (2) cT0–4 N0–3 M0 histopathologically proven squamous cell carcinoma of the oral cavity, oropharynx, hypopharynx, larynx, or unknown primary; (3) planned to undergo unilateral or bilateral neck dissection; and (4) providing informed consent. Exclusion criteria were (1) prior cervical radiotherapy and/or lymphadenectomy; (2) contraindications to USPIO; (3) contraindications to MRI; and (4) unable to provide informed consent.

USPIO-Enhanced In Vivo MRI

All patients received ferumoxtran-10 (Ferrotran; SPL Medical BV, Nijmegen, the Netherlands, investigational product) intravenously in weight-adapted dosage of 2.6 mg/kg body weight, 24 to 36 hours before the MRI scan as previously described.[24] Administration was performed under constant medical supervision over a period of 30 to 45 minutes. Magnetic resonance examinations were carried out on a 3 T MR system (Siemens Magnetom; Prisma, Erlangen, Germany) using a head and neck coil and a small flexible surface array coil covering the upper part of the thorax. Images of the cervical region extending from the base of skull to the manubrium sterni were obtained. Coronal turbo inversion recovery magnitude (TIRM) T2-weighted images, 3D Dixon volume interpolated gradient echo (VIBE) T1-weighted images, and 3D multigradient echo (MGRE) T2*-weighted images were acquired. Details of the specific pulse sequences are displayed in Table 1. T2* fits of individual pixels of the MGRE images were used to calculate computed echo time (cTE) images of 12 milliseconds to provide iron-sensitive contrast for interpretation of signal retention or attenuation within the identified lymph nodes.[25]

Initial In Vivo MRI Evaluation

The USPIO-enhanced MRIs were collectively read by 2 radiologists, of which one (P.Z.) has 8 years of experience in reading USPIO-enhanced MRIs and the other (S.A.H.P.) has 6 years of experience in reading head and neck MRIs. The T1 VIBE Dixon in-phase and T2 TIRM sequences were used to localize lymph nodes. The signal attenuation of these lymph nodes on the computed T2*-weighted MGRE image was used to identify lymph nodes with remaining signal intensity on iron-sensitive MRI. Nodes with any remaining signal intensity, such as an inhomogeneous appearance or signal intensity distribution, a high signal, or irregular shape, which could potentially be regarded suspicious for harboring metastatic deposits, were considered as potentially metastatic lymph nodes (PMLNs) and annotated on USPIO-enhanced MRI. All lymph nodes without any signal intensity on T2*-weighted MGRE sequence (eg, with homogenous uptake of USPIO) were regarded as on-imaging nonmetastatic lymph nodes (NMLNs).

Surgery

Local tumor resection and lymphadenectomy (neck dissection) were performed after USPIO-enhanced MRI, with a maximum interval between MRI and surgery of 7 days. The extent of neck dissection was based on local clinical guidelines. After surgery, the neck dissection specimen was pinned on a schematic drawing of the neck levels of which a digital photograph was taken (Fig. 1A). The surgical specimen was fixated in 10% buffered formalin for at least 12 hours.

Ex Vivo MRI Acquisition and Evaluation

We used an ex vivo MRI acquisition of the resected specimen as an essential aid to identify and match the location of in vivo identified lymph nodes in the resection specimen for node-to-node correlation of in vivo MRI and histopathology.[26] After fixation in formalin, the neck levels were separated to visualize the borders of the dissected neck levels on ex vivo MRIs (Figs. 1B–D). These separate levels were vacuum sealed in plastic (TissueSAFE plus device; Milestone, Sorisole, Italy) in their original configuration for optimal preservation and orientation (Fig. 1C), after which an ex vivo MRI was obtained (Fig. 1D).

All ex vivo MRIs were acquired on a preclinical 7.0 T MR system (Bruker ClinScan; BioSpin, Ettlingen, Germany) with gradient insert and an 86-mm body coil. The ex vivo MRI examinations consisted of a frequency-selective lipid excitation T1-weighted 3D GRE sequence and a frequency-selective water excitation 3D MGRE pulse sequence with 5 acquired echoes (Table 1). A lymph node was identified as a spherical and bordered structure in the transverse, sagittal, and coronal plane by combined reading of the water images (high signal intensity of nodes) and lipid selective images (absence of signal in nodes, Fig. 1D). As a next step, in vivo MRI PMLNs were matched and annotated to the ex vivo MRI (Fig. 2). Matching was based on the neck level, nodal size, and location in relation to anatomical landmarks, such as other lymph nodes, the submandibular gland, blood vessels, or the sternocleidomastoid muscle.

Histopathological Evaluation

The 3D images of ex vivo MRI including annotations of PMLN were present during the dissection of the specimen and guided the identification of the PMLN identified by USPIO-enhanced MRI. These were separately numbered, enclosed in a tissue cassette and sectioned on different levels, and stained with hematoxylin and eosin (HE) and CKPan AE immunohistochemical staining according to the standard head and neck sentinel node protocol. If a PMLN appeared obviously metastatic on macroscopy, standard histopathology with a single HE stain per slide was applied. On-imaging NMLNs were sectioned once, stained with HE, and processed per neck level as normal clinical workup.

Evaluation and Comparison of MRI With Histopathology

All matched PMLNs were compared with histopathology of the resected nodes, to identify MR signal properties discriminating between the presence and absence of metastases in these nodes. Two radiologists in consensus evaluated MRI signal intensity patterns for histologically positive and negative lymph nodes. Magnetic resonance criteria used for evaluation were hyperintensities, isointensities, or hypointensities of or in the PMLN and NMLN on calculated MGRE sequence (cTE of 12 milliseconds) when compared with the surrounding fat tissue,

TABLE 1. Overview of the In Vivo MRI and Ex Vivo MRI Parameters

	USPIO-Enhanced In Vivo MRI			Ex Vivo MRI	
	T2 TIRM (Inversion Time 230 ms)	T1 VIBE Dixon	T2* MGRE	Lipid Excitation	Water Excitation
Resolution, mm^3	0.8 × 1.0 × 4.0	0.8 × 0.8 × 0.8	0.8 × 0.8 × 0.7	0.2 × 0.2 × 0.2	0.2 × 0.2 × 0.2
Matrix	320 × 285 × 34	260 × 260 × 154	260 × 260 × 154	512 × 416 × 192	512 × 416 × 192
Acquisition mode	2D	3D	3D	3D	3D
Echo time, ms	64	2.57, 3.8	2.5–27.1	3	3
Repetition time, ms	5880	6.02	31	15	30
Bandwidth, Hz	237	300	360	320	320
Acquisition time, min	5:00	4:53	11:08	10:00	19:59
Flip angle, degrees	160*	10	10	10	14

*This is the refocusing flip angle in the fast spin echo train.

USPIO, ultrasmall superparamagnetic iron oxide; MRI, magnetic resonance imaging; TIRM, turbo inversion recovery magnitude; VIBE, volume interpolated gradient echo; MGRE, multigradient echo; 3D, 3-dimensional; 2D, 2-dimensional.

which correlated (or not) with the metastatic tissue deposits in the lymph nodes on histopathology.

RESULTS

Eleven patients were included in this study. In 1 patient, USPIO infusion was interrupted due to the onset of nausea and vomiting. These symptoms resolved partially after infusion was stopped. This patient seemed to have a medical history of malaise and daily frequent vomiting in the 2 weeks before USPIO infusion. The patient refused to restart the infusion and was therefore excluded from the study. The remaining 10 patients (mean age, 69 years; range, 52–78 years) were diagnosed with a primary tumor located in the oral cavity (n = 9) and oropharynx (n = 1). Baseline patient characteristics of these 10 patients are summarized in Table 2. The mean interval between USPIO infusion and MRI and USPIO infusion and surgery was 28 hours (range, 26–30) and 4 days (range, 2–5), respectively.

Image quality of the T1-weighted Dixon VIBE sequence was excellent in all 10 patients. Image quality of the T2*-weighted MGRE sequence varied among patients. Generally, quality was poorer in neck level I due to motion artifacts of the tongue. Nevertheless, analysis was not obstructed in nearly all neck levels in all patients since we used the Dixon VIBE for lymph node localization and assessed its signal intensity on the corresponding and matched T2* image.

Histopathological Findings

Histopathology revealed a total of 433 lymph nodes of which 411 were benign and 22 were malignant. The mean number of malignant nodes per patient was 2 (range, 0–8). Most metastases were observed in level II (n = 11), followed by level I (n = 6), level IV (n = 2), and level III (n = 1). The remaining 2 metastases were large, 65 mm and 75 mm, crossing boundaries between levels II and IV. The median size of the metastatic deposits excluding the 2 large metastases of 65 mm and 75 mm was 2.2 mm (range, 0.3–24 mm).

The resection specimen of patient 7 did not undergo ex vivo MRI as it was already processed at the dissection room for pathological workup. However, because all lymph nodes were found negative during histopathologic workup in this patient, a node-to-node correlation was not necessary to evaluate USPIO-enhanced MRI, and the material remained evaluable for the study.

Analysis of the Initial In Vivo USPIO-Enhanced MRI

In total, 35 PMLNs were identified by the radiologists on USPIO-enhanced MRI. These nodes were successfully matched to ex vivo MRI and histopathology on a node-to-node basis. Histopathology findings showed that 16 of these PMLNs were malignant (including the 2 exceptionally large metastases) and 19 were benign. Results of the analysis are schematically shown in Table 3. Six histopathologically

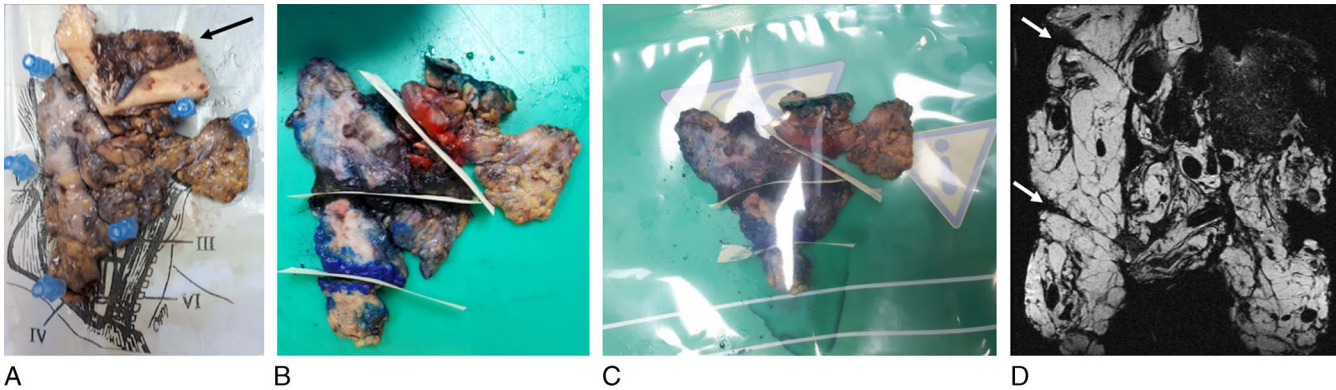

FIGURE 1. A, Example of a neck dissection specimen with the right-sided levels I–IV fixated in formalin. On the top, the resection of the primary tumor located in the jaw is visible (black arrow). B, The borders between the levels are inked (I–II: red, II–III: black, III–IV: blue), and a piece of article is placed in between. C, The specimen is put in a plastic bag and vacuum sealed. D, The borders between the levels on ex vivo MRI (lipid excitation) of the specimen are clearly visible (white arrows). The spherical structures with absence of MR signal intensity are lymph nodes.

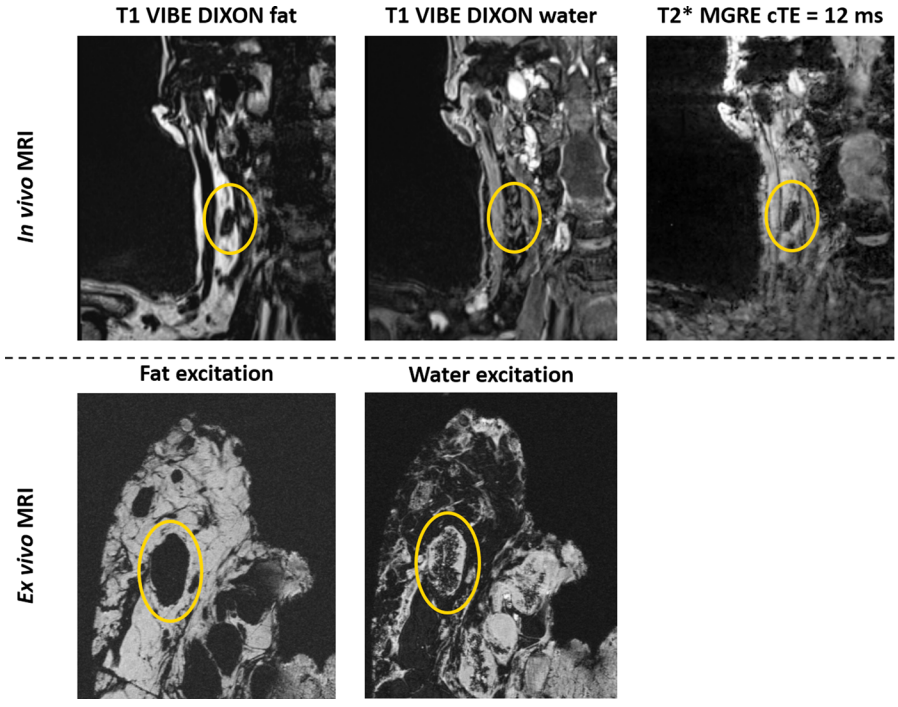

FIGURE 2. Visualization of an on-imaging potentially metastatic lymph node (PMLN) situated in neck level II on the right side on in vivo USPIO-enhanced MRI using T1 Dixon VIBE fat (top left) and water (top middle) images for anatomical localization and T2*-weighted MGRE MRI for interpretation of contrast enhancement (top right). Based on its location, size, and shape, the same PMLN is identified on ex vivo MRI of the excised neck specimen, consisting of a frequency-selective lipid excitation T1-weighted 3D GRE image (bottom left) and a frequency-selective water excitation 3D MGRE image (bottom right).

malignant lymph nodes were not identified as PMLN and could also in retrospect not be reliably identified on USPIO-enhanced MRI. Unfortunately, we did not discover whether these 6 lymph nodes were correlated to an NMLN or could not be detected at all on in vivo MRI. For pragmatic reasons, we have assumed that all 6 lymph nodes were correlated to an NMLN. It must be emphasized that this assumption portrays a worst-case scenario since the 6 lymph nodes could just have well been missed due to motion artifacts for example. The median size of the metastatic deposit within these 6 lymph nodes was 2 mm (range, 0.3–5 mm; Table 4).

USPIO-Enhanced MRI Pattern of Malignant and Benign Lymph Nodes: A Reading Algorithm

Radiological reassessment of T2*-weighted MGRE (cTE of 12 milliseconds) showed that 15/16 (94%) of the histopathologically

TABLE 2. Baseline Patient Characteristics

Patient	Sex	Age	Tumor Localization	Tumor Localization Specified	Tumor Side	pT	cN	pN	cM	Tumor Stage	Neck Levels Resected	
											Right	Left
1	Male	72	Oral cavity	Floor of mouth	Left	T3	N0	N0	M0	III	I–II	I–III
2	Male	52	Oral cavity	Floor of mouth	Left	T3	N0	N0	M0	III	I–III	I–III
3	Male	65	Oral cavity	Anterior tongue	Left	T2	N0	N2b	M0	IVa	—	I–III
4	Female	78	Oropharynx*	Base of tongue	Left	T2	N3	N3	M0	II	—	IB–V
5	Male	64	Oral cavity	Floor of mouth	Midline	T3	N2c	N3b	M0	IVb	I–III	I–IV
6	Male	72	Oral cavity	Floor of mouth	Right	T1	N3	N3	M0	IVb	II–V	—
7	Female	69	Oral cavity	Floor of mouth	Midline	T3	N0	N0	M0	III	I–III	I–III
8	Male	67	Oral cavity	Floor of mouth	Left	T3	N0	N2b	M0	IVa	—	I–III
9	Male	75	Oral cavity	Lower alveolus	Right	T4a	N0	N2b	M0	IVb	I–IV	—
10	Female	72	Oral cavity	Lower alveolus	Left	T4a	N0	N0	M0	IVa	—	I–III

Tumor stage was classified using the eighth edition TNM Classification of Malignant Tumors of the Union for International Cancer Control.

*HPV-positive tumor.

P, pathologic; T, tumor; N, node; c, clinical, M, metastasis.

TABLE 3. An Overview Demonstrating the Number of Histopathologically Proven Lymph Nodes and Summarizing the Results of Analysis of In Vivo USPIO-Enhanced MRI on a Patient Level

Patient	No. HP Proven Positive LN	No. PMLN on USPIO-Enhanced MRI	No. PMLN Positive on HP	No. PMLN Positive on HP With an Equal or Higher Signal Intensity on T2* MGRE	No. PMLN Negative on HP	No. PMLN Negative on HP With a Lower Signal Intensity on T2* MGRE	No. HP Positive LN Not Detected by USPIO-Enhanced MRI
1	0	0	0	—	0	0	0
2	0	2	0	—	2	1*	0
3	2	1	1	1	0	0	1
4	2	3	2	2	1	0*	0
5	8	5	5	5	0	0	3
6	3	2	2	2	0	0	1
7	0	5	0	—	5	5	0
8	4	4	3	2	1	1	1
9	3	6	3	3	3	3	0
10	0	7	0	—	7	7	0
Total	22	35	16	15	19	17	6

The (other) PMLN that appeared negative on histopathology still had an equal or high signal intensity on T2-weighted MGRE after application of the reading algorithm.

USPIO, ultrasmall superparamagnetic iron oxide; MRI, magnetic resonance imaging; HP, histopathology; LN, lymph nodes; PMLN, potentially metastatic lymph node.

malignant lymph nodes (median size of the metastatic deposit of 6.5 mm; range, 1–75 mm) displayed an equal or higher signal MRI intensity when compared with lipid tissue (Fig. 3A). One lymph node did not show an equal or higher signal intensity when compared with lipid tissue (the diameter of the metastatic deposit was 0.4 mm, Fig. 3B).

Of the 19 MRI-suspicious (PMLN) but histopathologically benign lymph nodes, 17 (89%) displayed a lower, often heterogenous, MRI signal intensity when compared with lipid tissue on T2*-weighted MGRE cTE of 12 milliseconds (Fig. 3C). The 2 remaining negative lymph nodes both showed a focal increased signal intensity. One of these (Fig. 3D) was punctured under ultrasound guidance 14 days before in vivo USPIO-enhanced MRI, which might have caused a small hematoma. The other lymph node (Fig. 3E) showed an area of fibrosis.

When compared with the existing reading algorithm that was used to identify PMLNs, the new reading algorithm brought the amount of false-positives down from 19/35 to 2/17, and the amount of true-positives up from 16/35 to 15/16.

A total of 279 lymph nodes showed complete attenuation of signal intensity on T2*-weighted MGRE cTE of 12 milliseconds and were thus regarded as NMLN. Of these, 273 (98%) were actually benign and were correlated on an neck level basis to histopathology, which revealed 392 negative lymph nodes.

Summarizing our results, we can conclude that on USPIO-enhanced MRI on T2*-weighted MGRE (cTE of 12 milliseconds) imaging, histopathologically malignant lymph nodes display an equal or higher signal intensity when compared with lipid tissue, whereas histopathologically benign lymph nodes display a lower signal intensity or complete loss of signal. This led to our new reading algorithm, schematically represented in Figure 4 (Supplementary Digital Content, http://links.lww.com/RLI/A727).

TABLE 4. Size of Metastatic Deposit and Lymph Node Regarding the 6 Histopathologically Proven Positive Lymph Nodes That Could Not Be Found on In Vivo USPIO-Enhanced MRI

Lymph Node	Largest Diameter of Metastatic Deposit, mm	Long Axis Diameter of Lymph Node, mm	Short Axis Diameter of Lymph Node, mm
1	0.5	14	7.2
2	5.0	7.2	5.4
3	3.5	4	3
4	2.0	2	1
5	2.5	6.9	4.8
6	0.3	7.9	5.7

USPIO, ultrasmall superparamagnetic iron oxide; MRI, magnetic resonance imaging.

DISCUSSION

In head and neck cancer patients, evaluation of lymph node status is performed by palpation and imaging techniques such as MRI, CT, ultrasound, and US-guided fine-needle cytology that rely merely on nodal size and shape. The limited sensitivity of these parameters accounts for unsatisfactory performance of conventional imaging and urges the need for modalities assessing other features that provide a differentiation between a benign and metastatic (part of a) lymph node.[27] Improved nodal metastasis detection provides an opportunity for safe minimization of elective neck treatment on an individual patient basis.[19] Reduction of the elective neck radiation dose or volume contributes to a significant lower dysphagia and salivary gland toxicity rate, and is thus of major clinical relevance.[28–30] The present study was designed to determine the distinctive imaging features on USPIO-enhanced MRI using modern 3D MR techniques with a high spatial resolution to discriminate malignant from benign lymph nodes in head and neck cancer patients. Our workflow incorporating an ex vivo MRI of the neck dissection specimen enabled a node-to-node correlation with histopathology of suspicious lymph nodes, from which we were able to derive in vivo signal intensity properties differentiating between benign and malignant nodes. As the time between USPIO infusion and surgery varied between patients (4 days on average), we did not evaluate the presence of remaining USPIO in the ex vivo scans. The purpose of these scans was to identify and match lymph nodes for the node-to-node correlation, not for the presence or absence of USPIO nanoparticles. A large proportion (94%, 15/16) of the PMLN and histopathologically malignant lymph nodes show an equal or higher signal intensity when

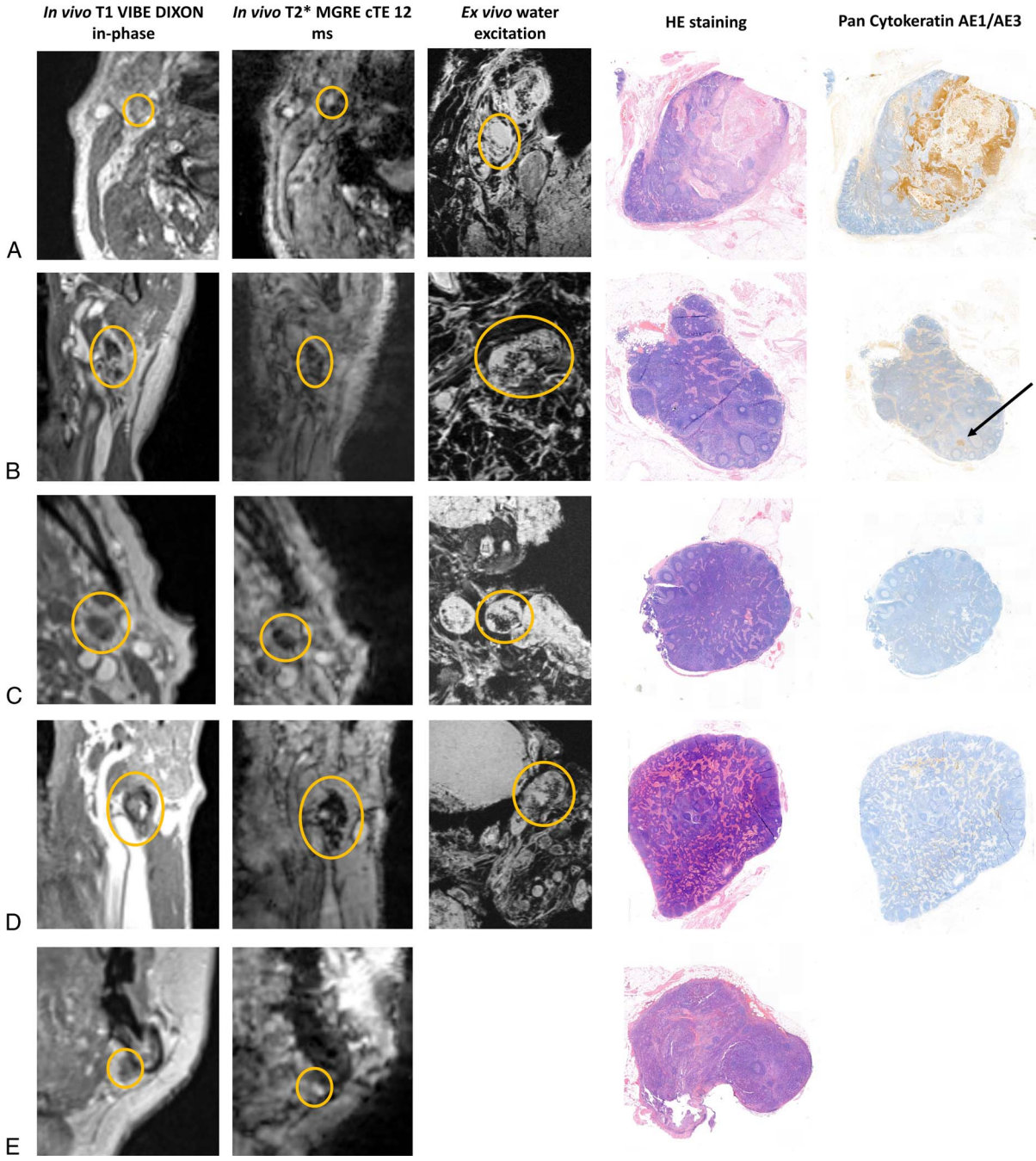

FIGURE 3. Examples of in vivo T1 Dixon VIBE, T2*-weighted MGRE cTE of 12 milliseconds, ex vivo water excitation, hematoxylin and eosin staining and immunohistochemistry staining with Pan Cytokeratin AE1/AE3 in A, an on-imaging potentially metastatic (due to a higher signal MRI intensity when compared with lipid tissue on T2*-weighted MGRE) and pathology positive lymph node, B, an on imaging nonmetastatic (due to a heterogenous lower signal MRI intensity when compared with lipid tissue on T2*-weighted MGRE) and pathology positive lymph node with a metastatic deposit of 0.4 mm, C, an on imaging nonmetastatic (due to an absent signal MRI intensity on T2*-weighted MGRE) and pathology negative lymph node, and D and E, each the 2 on-imaging potentially metastatic (due to a focal higher signal MRI intensity when compared with lipid tissue on T2*-weighted MGRE) and pathology negative lymph node, one with a possible hematoma and one with fibrosis.

compared with lipid tissue on a T2*-weighted MGRE sequence with a cTE of 12 milliseconds. Furthermore, 89% (17/19) of the PMLN and histopathologically benign lymph nodes matched on a node-to-node basis showed a lower or no signal intensity when compared with lipid tissue. At least 98% (273/279) of the NMLNs, matched on a neck level basis, were histopathologically benign. Six histopathologically proven positive lymph nodes were not identified on USPIO-enhanced MRI as potentially suspect for metastases.

Several studies have investigated the correlation between radiographic features and histopathology of lymph nodes on USPIO-enhanced MRIs. In a study conducted by Harisinghani et al,[22] it was shown that in pelvic and abdominal lymph nodes >10 mm, T2 and T2*-weighted MR

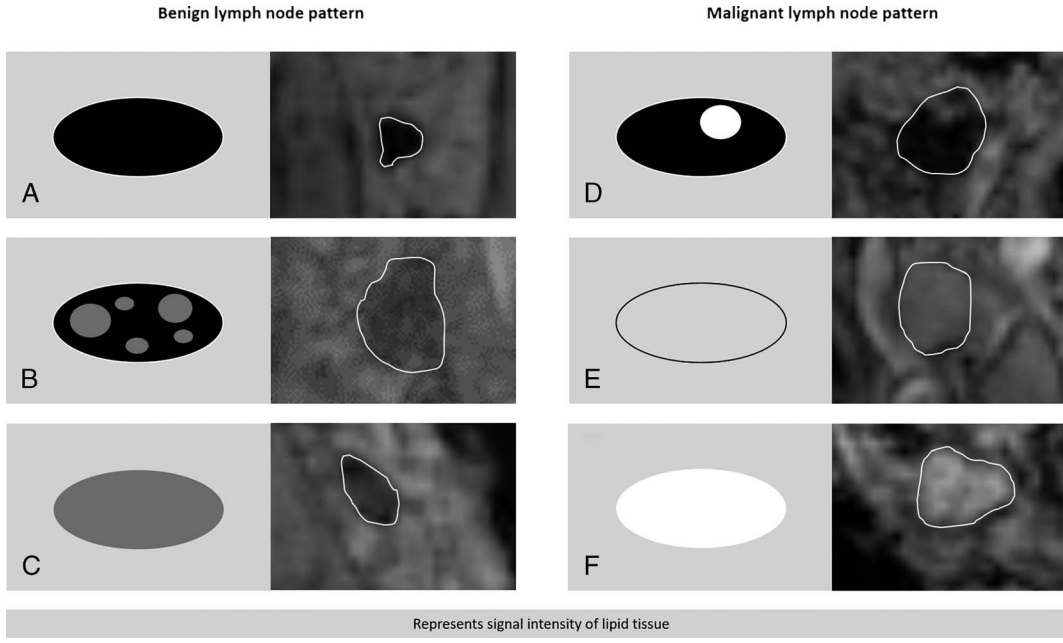

FIGURE 4. Schematic representation of the reading algorithm. Lymph nodes displaying a uniform absent (A), heterogenous (B), or lower (C) signal intensity when compared with the surrounding subcutaneous fat on T2*-weighted MGRE with a computed TE of 12 milliseconds are regarded as negative (benign lymph node pattern). Lymph nodes displaying a partial high (D), equal (E), or higher (F) signal intensity when compared with the surrounding subcutaneous fat on T2*-weighted MGRE with a computed TE of 12 milliseconds are regarded as positive (malignant lymph node pattern).

signal intensity was maintained in 93% of the malignant lymph nodes and decreased in 100% of benign lymph nodes, corroborating our results. However, MRIs were acquired on a 1.5 T system in 2D mode using a slice thickness of 8 mm, and the lymph nodes included in the analysis had a large mean size of 14 mm. In the current study, high-resolution MR images with 3D isotropic resolution of 0.8 mm were acquired on a 3 T MR system, reliably visualizing lymph nodes down to approximately 1 to 2 mm in size. Other researchers have investigated the nodal pattern on T2*-weighted USPIO-enhanced MRI in rectal cancer patients and reported that a uniform and central low signal intensity characterizes benign and inflammatory lymph nodes. On the contrary, an eccentric and a uniform high signal intensity characterizes malignant lymph nodes.[23] Examinations were performed in 2D mode on a 1.5 T MR system with a slice thickness of 3 mm. Another study investigated evaluation of mesorectal lymph nodes of rectal cancer on USPIO-enhanced MRI for qualitative characteristics (border irregularities, short- and long-axis diameter, and estimated percentage [<30%, 30%–50%, or 50%] of high signal intensity region) and one quantitative parameter (ratio of high signal intensity region within the lymph node). Their findings showed a sensitivity of 93% and specificity of 96% for accurately staging a lymph node as malignant when the estimated percentage of high signal intensity region exceeded 30%.[21] Very recently, using an almost binary distinction between absence and presence of signal intensity in mesorectal lymph nodes resulted in lower accuracy in staging rectal cancer with high-resolution 3D USPIO-MRI.[4] These rectum studies provide further support for our results, demonstrating that reading USPIO-enhanced MRIs requires a more differentiated approach rather than merely observing a difference between the absence and presence of signal intensity of the whole lymph node. Moreover, the location of lymph nodes in the body (mesorectum, pelvis, or neck) could cause differences in USPIO accumulation in these nodes, illustrating perhaps a need for region-specific adaptation of USPIO-MRI reading algorithms.

We anticipated that USPIO uptake in cervical lymph nodes can be altered due to an increased exposure to infections of the upper aerodigestive tract. Reactive changes such as hyperplasia of germinal centers, hyaline metamorphosis, sinus histiocytosis, and fibrosis can result in a lack of cells of the mononuclear phagocyte system causing no or limited USPIO uptake.[18] Consequentially, some MR signal intensity is maintained on T2*-weighted MRI and a positive lymph node may be mimicked. The findings of the current study, however, suggest that this can be overcome with the presented reading algorithm. There were only 2 histopathologically proven negative lymph nodes that displayed an area of high signal intensity. One lymph node was punctured during routine diagnostics, which can have altered USPIO uptake. Because small hematomas are not visible on histopathological slides, we could not actually prove this, although the theory seems reasonable. The configuration of the other lymph node was indeed modified by fibrotic tissue.

Six histopathologically proven positive lymph nodes were not identified on USPIO-enhanced MRI as potentially suspect for metastases. Retrospective localization on MRI of these lymph nodes based on size, enhancement pattern, and nodal neck station failed. As the median diameter of the metastatic area was only 2 mm (range, 0.3–5 mm), these lymph nodes likely did not show the distinctive malignant appearance on USPIO-enhanced MRI and were therefore missed. The lymph node with a metastatic deposit of 5 mm was located in neck level I in a patient where MRI quality was poor due to severe motion artifacts. For this reason, the lymph node was not visible at all.

Our reading algorithm uses a T2*-weighted MGRE sequence without fat suppression to compare MRI signal intensities of lymph nodes and their surrounding fat. Not suppressing fat leaves high MR signal of fat, whereas the MR signal of a malignant lymph node embedded in the lipid tissue also remains high. Identification of a malignant, that is, "white" node in "white" surrounding tissue can be challenging and therefore a potential source of error. We solved this by adding T1-weighted VIBE Dixon MR sequences for anatomical localization of all lymph nodes to the MR protocol. Reading the images was, however, labor intensive and time-consuming. Nevertheless, its potential ability to de-escalate elective neck irradiation and surgery outweighs this disadvantage.

A frequently used imaging tool for N-staging in this group of patients is FDG PET/CT, and its accuracy is well described in literature. In a meta-analysis, the pooled sensitivity and specificity with 95% confidence interval for PET/CT on a per-neck-side analysis were 0.84 (0.77–0.89) and 0.84 (0.78–0.89).[31] The corresponding values for PET/CT on a per-nodal-level analysis were 0.84 (0.78–0.88) and 0.96 (0.94–0.98). Even if our study was not intended to validate the USPIO-enhanced MRI in detection of metastatic lymph nodes, we can provide a first preliminary look into the accuracy of the new reading algorithm. With high-resolution 3D USPIO-enhanced MRI, 15/16 (94%) metastatic lymph nodes showed equal or higher MRI signal intensity when compared with lipid tissue on T2*-weighted MRI, whereas 17/19 (89%) healthy lymph nodes showed lower attenuation of signal intensity when compared with lipid tissue on T2*-weighted MRI. A total of 279 NMLNs matched on a neck level basis showed complete attenuation of signal intensity when compared with lipid tissue of which 273 (98%) were actually benign. These numbers are based on node-to-node matching, as opposed to neck level or neck side for FDG PET/CT. A follow-up validation study with more patients is needed to provide more insight on the accuracy of USPIO-enhanced MRI.

An obvious limitation of this study is the small number of patients. Although many lymph nodes were visible on MRI and harvested with MR-guided histopathology, the new algorithm is based on a limited number of positive lymph nodes. However, all these nodes were matched node-to-node from histopathology to in vivo MRI, providing a solid ground truth. Another limitation was the absence of node-to-node correlation for all MRI negative lymph nodes (NMLNs), due to the sheer amount of lymph nodes per neck dissection specimen (average of 31 lymph nodes per specimen per side). Nevertheless, data from a previous study in rectal cancer that attempted a node-to-node correlation of all lymph nodes show that only 40% of the nodes detected with ex vivo MRI were actually retrieved in the dissection specimen.[32] Therefore, we opted for a correlation on a nodal basis for the PMLNs and on a neck level basis for the NMLNs. The location of a PMLN in relation to anatomical landmarks was used to match these nodes to ex vivo MRI, serving as guidance for nodal histopathology during step-sectioning. For this reason, PMLNs were relatively easy to localize in the dissection specimen. Neck level-to-level correlation of the NMLN around the exactly matched nodes was therefore relatively simple. A final limitation is the use of weighted signal intensities rather than quantitative MR biomarkers (eg, T1, T2, or T2* values) for the differentiation between benign and malignant nodes. The current algorithm is based on 3 T MGRE measurements with a cTE of 12 milliseconds and a repetition time and flip angle of 31 milliseconds and 10 degrees. If in a prospective study this algorithm lives up to its promise, more exact quantification of T1 and T2* relaxation times can make the algorithm more generalizable to other MR protocol settings on different systems.

In conclusion, we developed a reading algorithm for differentiation between malignant and benign cervical lymph nodes in head and neck cancer patients on T2*-weighted USPIO-enhanced MRI using histopathology as the criterion standard. With the used protocol at a magnetic field strength of 3 T, an equal or higher signal intensity compared with surrounding lipid tissue on a T2*-weighted MGRE sequence characterizes a metastatic lymph node (or partial intranodal metastasis), whereas a lower signal intensity when compared with lipid tissue features a healthy or benign lymph node. Together with high-resolution 3D MRI, this reading algorithm allows the detection of small metastatic (parts of) lymph nodes with less false-positives when compared with traditional interpretation of USPIO-enhanced MRI. This reading algorithm is now ready to be tested in larger-scale prospective clinical studies predicting lymph node status in individual lymph nodes of patients with head and neck cancer using USPIO-enhanced MRI.

REFERENCES

1. Woolgar JA. Histopathological prognosticators in oral and oropharyngeal squamous cell carcinoma. *Oral Oncol*. 2006;42:229–239.
2. Schilling C, Stoeckli SJ, Haerle SK, et al. Sentinel European Node Trial (SENT): 3-year results of sentinel node biopsy in oral cancer. *Eur J Cancer*. 2015;51:2777–2784.
3. Sanabria A, Shah JP, Medina JE, et al. Incidence of occult lymph node metastasis in primary larynx squamous cell carcinoma, by subsite, T classification and neck level: a systematic review. *Cancers (Basel)*. 2020;12:1059.
4. Stijns RCH, Philips BWJ, Nagtegaal ID, et al. USPIO-enhanced MRI of lymph nodes in rectal cancer: a node-to-node comparison with histopathology. *Eur J Radiol*. 2021;138:109636.
5. Schilham MGM, Zamecnik P, Prive BM, et al. Head-to-head comparison of (68) Ga-prostate-specific membrane antigen PET/CT and ferumoxtran-10-enhanced MRI for the diagnosis of lymph node metastases in prostate cancer patients. *J Nucl Med*. 2021;62:1258–1263.
6. Fortuin AS, Bruggemann R, van der Linden J, et al. Ultra-small superparamagnetic iron oxides for metastatic lymph node detection: back on the block. *Wiley Interdiscip Rev Nanomed Nanobiotechnol*. 2018;10.
7. de Gouw D, Maas MC, Slagt C, et al. Controlled mechanical ventilation to detect regional lymph node metastases in esophageal cancer using USPIO-enhanced MRI; comparison of image quality. *Magn Reson Imaging*. 2020;74:258–265.
8. Weissleder R, Elizondo G, Wittenberg J, et al. Ultrasmall superparamagnetic iron oxide: characterization of a new class of contrast agents for MR imaging. *Radiology*. 1990;175:489–493.
9. Harisinghani MG, Barentsz J, Hahn PF, et al. Noninvasive detection of clinically occult lymph-node metastases in prostate cancer. *N Engl J Med*. 2003;348:2491–2499.
10. Heesakkers RA, Hovels AM, Jager GJ, et al. MRI with a lymph-node-specific contrast agent as an alternative to CT scan and lymph-node dissection in patients with prostate cancer: a prospective multicohort study. *Lancet Oncol*. 2008;9:850–856.
11. Baghi M, Mack MG, Hambek M, et al. The efficacy of MRI with ultrasmall superparamagnetic iron oxide particles (USPIO) in head and neck cancers. *Anticancer Res*. 2005;25:3665–3670.
12. Mack MG, Balzer JO, Straub R, et al. Superparamagnetic iron oxide-enhanced MR imaging of head and neck lymph nodes. *Radiology*. 2002;222:239–244.
13. Sigal R, Vogl T, Casselman J, et al. Lymph node metastases from head and neck squamous cell carcinoma: MR imaging with ultrasmall superparamagnetic iron oxide particles (Sinerem MR)—results of a phase-III multicenter clinical trial. *Eur Radiol*. 2002;12:1104–1113.
14. Curvo-Semedo L, Diniz M, Migueis J, et al. USPIO-enhanced magnetic resonance imaging for nodal staging in patients with head and neck cancer. *J Magn Reson Imaging*. 2006;24:123–131.
15. Hoffman HT, Quets J, Toshiaki T, et al. Functional magnetic resonance imaging using iron oxide particles in characterizing head and neck adenopathy. *Laryngoscope*. 2000;110:1425–1430.
16. Anzai Y, Piccoli CW, Outwater EK, et al. Evaluation of neck and body metastases to nodes with ferumoxtran 10-enhanced MR imaging: phase III safety and efficacy study. *Radiology*. 2003;228:777–788.
17. Baghi M, Mack MG, Wagenblast J, et al. Iron oxide particle-enhanced magnetic resonance imaging for detection of benign lymph nodes in the head and neck: how reliable are the results? *Anticancer Res*. 2007;27:3571–3575.
18. Wensing BM, Deserno WM, de Bondt RB, et al. Diagnostic value of magnetic resonance lymphography in preoperative staging of clinically negative necks in squamous cell carcinoma of the oral cavity: a pilot study. *Oral Oncol*. 2011;47:1079–1084.
19. Driessen D, Dijkema T, Weijs WLJ, et al. Novel diagnostic approaches for assessment of the clinically negative neck in head and neck cancer patients. *Front Oncol*. 2020;10:637513.
20. Scheenen TWJ, Zamecnik P. The role of magnetic resonance imaging in (future) cancer staging: note the nodes. *Invest Radiol*. 2020;56:42–49.
21. Lahaye MJ, Engelen SM, Kessels AG, et al. USPIO-enhanced MR imaging for nodal staging in patients with primary rectal cancer: predictive criteria. *Radiology*. 2008;246:804–811.
22. Harisinghani MG, Saini S, Weissleder R, et al. MR lymphangiography using ultrasmall superparamagnetic iron oxide in patients with primary abdominal and pelvic malignancies: radiographic-pathologic correlation. *AJR Am J Roentgenol*. 1999;172:1347–1351.
23. Koh DM, Brown G, Temple L, et al. Rectal cancer: mesorectal lymph nodes at MR imaging with USPIO versus histopathologic findings—initial observations. Radiology 2004;231:91–9.

24. Hudgins PA, Anzai Y, Morris MR, et al. Ferumoxtran-10, a superparamagnetic iron oxide as a magnetic resonance enhancement agent for imaging lymph nodes: a phase 2 dose study. *AJNR Am J Neuroradiol*. 2002;23:649–656.
25. Philips BWJ, Fortuin AS, Orzada S, et al. High resolution MR imaging of pelvic lymph nodes at 7 Tesla. *Magn Reson Med*. 2017;78:1020–1028.
26. Driessen DAJJ, de Gouw DJJM, Stijns RCH, et al. Validation of in vivo nodal assessment of solid malignancies with USPIO-enhanced MRI: a workflow protocol. *Methods Protoc*. 2022;5:24.
27. Anzai Y, Brunberg JA, Lufkin RB. Imaging of nodal metastases in the head and neck. *J Magn Reson Imaging*. 1997;7:774–783.
28. de Veij Mestdagh PD, Walraven I, Vogel WV, et al. SPECT/CT-guided elective nodal irradiation for head and neck cancer is oncologically safe and less toxic: a potentially practice-changing approach. *Radiother Oncol*. 2020;147:56–63.
29. Nevens D, Duprez F, Daisne JF, et al. Reduction of the dose of radiotherapy to the elective neck in head and neck squamous cell carcinoma; a randomized clinical trial. Effect on late toxicity and tumor control. *Radiother Oncol*. 2017;122:171–177.
30. Nuyts S, Lambrecht M, Duprez F, et al. Reduction of the dose to the elective neck in head and neck squamous cell carcinoma, a randomized clinical trial using intensity modulated radiotherapy (IMRT). Dosimetrical analysis and effect on acute toxicity. *Radiother Oncol*. 2013;109:323–329.
31. Yongkui L, Jian L, Wanghan, et al. ^{18}FDG-PET/CT for the detection of regional nodal metastasis in patients with primary head and neck cancer before treatment: a meta-analysis. *Surg Oncol*. 2013;22:e11–e16.
32. Stijns R, Philips B, Wauters C, et al. Can ex vivo magnetic resonance imaging of rectal cancer specimens improve the mesorectal lymph node yield for pathological examination? *Invest Radiol*. 2019;54:645–652.